Fast-Ion Transport Induced by Alfven Eigenmodes in ASDEX Upgrade

M. Garcia-Munoz 1), I.G.J. Classen 2), B. Geiger 1), W.W. Heidbrink 3), M.A. Van Zeeland 4), S. Äkäslompolo 5), R. Bilato 1), V. Bobkov 1), M. Brambilla 1), S. da Graça 6), V. Igochine 1), Ph. Lauber 1), M. Maraschek 1), F. Meo 7), M. Schneller 1), G. Tardini 1),
and the ASDEX Upgrade Team

1) Max-Planck-Institut für Plasmaphysik, EURATOM Association, Garching, Germany
2) FOM-Institute for Plasma Physics Rijnhuizen, EURATOM Association, The Netherlands
3) University of California-Irvine, Irvine, CA 92697, USA
4) General Atomics, San Diego, CA 92186-5608, USA
5) Helsinki Univ. of Technology, Association EURATOM-TEKES, Finland
6) CFN, EURATOM Association-IST Lisbon, Portugal
7) Riso, EURATOM Association-RIS, Roskilde, Denmark

e-mail: Manuel.Garcia-Munoz@ipp.mpg.de

Abstract.
A comprehensive suite of diagnostics has allowed detailed measurements of the AE spatial structure and subsequent fast-ion transport. RSAEs and TAEs have been driven unstable by fast-ions from ICRH as well as NBI origin. In ICRF heated plasmas, diffusive and convective fast-ion losses induced by AEs have been characterized in fast-ion phase-space. While single RSAEs and TAEs eject resonant fast-ions in a convective process directly proportional to the fluctuation amplitude, $\delta B/B$, the overlapping of multiple RSAE and TAE spatial structures and wave-particle resonances leads to a large diffusive loss, scaling as $(\delta B/B)^2$. In beam heated discharges, coherent fast-ion losses have been observed primarily due to TAEs. Core localized, low amplitude NBI driven RSAEs have not been observed to cause significant coherent fast-ion losses. The temporal evolution of the confined fast-ion profile in the presence of RSAEs and TAEs has been monitored with high spatial and temporal resolution. A large drop in the central fast-ion density due to many RSAEs has been observed as q_{min} passes through an integer. The AE radial and poloidal structures have been obtained with unprecedented details using a fast SXR as well as 1D and 2D ECE radiometers. HAGIS simulations have been performed to investigate the transport mechanisms.

1. Introduction

Future burning plasma experiments such as ITER may be subject to the excitation of Alfven eigenmode (AE) instabilities [1] by 3.5 MeV fusion born alpha particles as well as fast-ions created by auxiliary heating systems. If allowed to grow unabated, these instabilities have the potential to cause fast-ion redistribution and loss leading to a degradation of the fusion performance, heating and current drive efficiencies as well as to possible serious damage of first wall components [2]. On the road to address these issues, significant progress in fast-ion physics has been made recently on ASDEX Upgrade (AUG). An extended suite of diagnostics now allows detailed measurements of AE spatial structure and the subsequent fast-ion transport. Fast 1D and 2D imaging [3] Electron Cyclotron Emission (ECE) measurements of the temperature fluctuations induced by the AEs have delivered unprecedented details on eigenmode radial and poloidal structure. The internal redistribution and loss of energetic particles in the presence of AEs have been measured with the Fast-Ion Loss Detectors (FILDs) [4] and the recently developed Fast-Ion D-Alpha (FIDA) spectroscopy [5]. During the past two years, experiments have been conducted in AUG to study the fast-ion transport due to AEs in plasmas heated purely by ICRH and NBI. In ICRH heated plasmas, strong fast-ion losses induced by RSAEs and TAEs have been observed [6]. Time-resolved energy and pitch angle measurements of fast-ion losses correlated in frequency and phase with RSAEs and TAEs have allowed clear identification of

the loss mechanisms. In NBI heated plasmas, RSAEs and TAEs have been driven unstable during the current ramp-up phase. Core localized, low amplitude NBI driven RSAEs have not been observed to cause significant coherent fast-ion losses. The fast-ion redistribution due to RSAEs and TAEs has been measured using the recently developed FIDA spectroscopy.

2. AEs and fast-ion transport in ICRF heated discharges

An important difference between present experiments and ITER will be the presence of fusion born α-particles as main heating source. MeV α-particles with relative small characteristic orbit lengths (compared to plasma minor radius), velocities well above the Alfven velocity and an isotropic distribution function will likely excite meso-scale fluctuations. In contrasts, in present experiments, fast-ions are mainly generated by external heating systems with highly anisotropic distribution functions that typically excite macro-scale collective modes (e.g. AEs). While RF heating systems mostly populate the fast-ion phase-space corresponding to deeply trapped supra-alfvenic ions, NBI systems, depending on their injection geometries, mainly create a large population of supra-thermal (in some cases even supra-alfvenic) passing-ions. In general, minority and high-harmonic RF heating constitute a unique tool to achieve some burning-relevant dynamical regimes with ions in the MeV range.

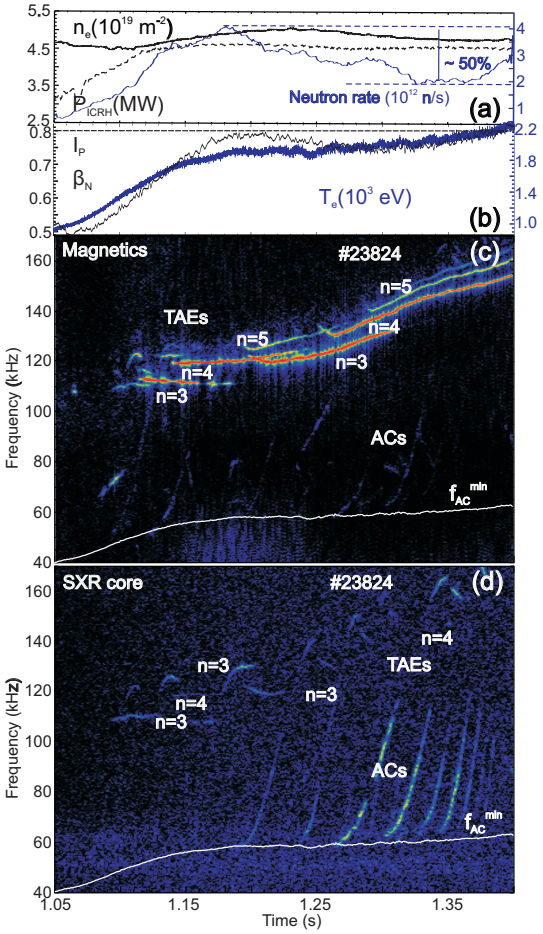

FIG. 1: AUG discharge #23824. (a) Core line integrated electron density, n_e, neutron rate and ICRH power (dashed line), P_{ICRH}. (b) Local core electron temperature, T_e, plasma current (dashed line), I_P, and normalized beta, β_N. (c) Spectrogram of an in-vessel magnetic pickup coil. (d) Spectrogram of a core SXR channel.

2.1. AEs

In AUG, on-axis minority RF heating in low density deuterium plasmas create a large population of supra-alfvenic ions that usually drive a rich variety of Alfven/Alfven-acoustic eigenmodes [7]. The experiments discussed here have been performed in plasmas with plasma current $I_p \approx 0.8\ MA$, toroidal field $B_t = 2.0\ T$, safety factor at the edge $q_{95} \approx 4.0$ and Ion Cyclotron Resonance Heating (ICRH) as main heating and fast particle source. 4.5 MW of on axis ICRF hydrogen minority heating was applied to a deuterium plasma ($n_H/n_D \approx 5\%$). Fig.1-(a) and -(b) show the main plasma parameters of the baseline discharge, #23824. Fig.1(c) and Fig.1(d) show, respectively, the Fourier spectrogram for a magnetic fluctuation signal and for a SXR signal, corresponding to a line of sight passing through the plasma core. Several coherent MHD fluctuations are visible around 110 kHz up to 170 kHz. They correspond to TAEs with different toroidal mode numbers, $n = 3, 4, 5$, as obtained from Mirnov coils, whose presence is confirmed also by comparison with ideal MHD calculations carried out with the NOVA code [8]. Magnetic fluctuations chirping in frequency from ≈ 50 kHz up to the

TAE frequencies (barely visible in the magnetics spectrogram) have been identified as ACs by means of the SXR emission from the plasma core as Fig.1(d) shows. The lowest AC frequency, f_{AC}^{min}, in Fig.1-(c) and -(d) is mainly given by the geodesic compressibility and the toroidal coupling to the acoustic waves, as expected by the theory [9]. Pressure effects modify the local dispersion relation for shear Alfvén waves in low-β plasmas: $\omega_{AC} \approx \left|\frac{m}{q_{min}-n}\right| \cdot \frac{V_A}{R_0}$, with m the poloidal mode number. The modified minimum of the local dispersion relation is then given by $\omega_{AC}^{min} \approx \frac{\sqrt{2}}{R_0} \cdot C_s = \frac{\sqrt{2}}{R_0} \cdot \left(\frac{T_i}{m_i}\right)^{1/2} \cdot \left(\frac{7}{4} + \frac{T_e}{T_i}\right)^{1/2}$. An excellent agreement between the experimental lowest AC frequency and the modified dispersion relation is clearly visible in Fig.1-(c) and -(d) (superimposed in white). The estimated f_{AC}^{min} has been calculated assuming $T_e = T_i$ and taking T_e from an ECE channel near the AC localization and assuming a neglectable plasma rotation.

Fluctuations in the electron temperature profile caused by the ACs and TAEs [10] have been measured with the 1D ECE radiometer. The AC and TAE radial structures have been reconstructed by means of ECE-FILD cross-correlation techniques to improve signal-to-noise ratios. Fig.2 shows the normalized crosspower spectral densities (coherence) as a function of ρ_{pol} and frequency for 50 ms time intervals. The AC and TAE radial structures were obtained by selecting and averaging a certain frequency band of the coherence. The selected AC and TAE frequency bands are given in Fig.2. Fig.2(a) shows global TAEs extended from $\rho_{pol} \approx 0.23$ up to the edge with broad ACs localized at $\rho_{pol} \approx 0.4$. A complete overlapping of AC-TAE radial structures is clearly visible (highlighted in yellow). Fig.2(b) shows the AC-TAE radial structures for a later time interval. TAEs shift outwards becoming more localized while ACs shift inwards becoming also more localized at $\rho_{pol} \approx 0.3$. The overlapping region becomes smaller. Finally, Fig.2(c) shows a neglectable AC-TAE spatial overlapping with ACs and TAEs well localized at $\rho_{pol} \approx 0.3$ and $\rho_{pol} \approx 0.6$ respectively. The largest ACs and TAEs presented here caused a normalized T_e perturbation of $\delta T_e/T_e \approx 0.009$.

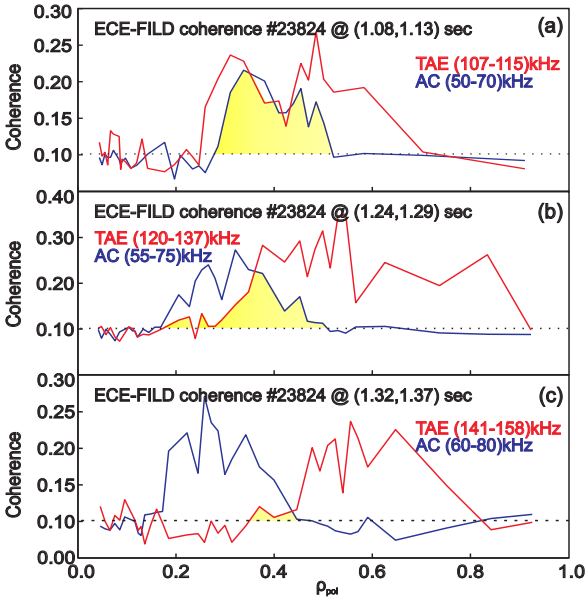

FIG. 2: AUG discharge #23824. ACs and TAEs radial structures obtained by means of ECE-FILD cross-correlation. AC radial structures are reconstructed at the AC lowest frequency. Different time intervals are displayed; (a) for (1.08-1.13) sec, (b) for (1.24-1.29) sec and (c) for (1.32, 1.37) sec. In yellow are highlighted the regions with overlapping TAE-AC internal structures well before the AC-TAE transition.

2.2. Fast-ion transport

A minimum RF power of ≈ 3 MW for on-axis minority heating is typically necessary in AUG to drive AEs unstable with energetic ions [11]. In the presence of ICRH driven RSAEs and TAEs strong fast-ion losses are detected by the FILD system [4] correlated with a neutron drop of ≈ 50 %, see Fig.1(a). According to ICRH simulations performed with the TORIC full-wave code [12], about 10% of the ICRH power is absorbed in this discharge directly by deuterium ions at the second harmonic ($\omega = 2\Omega_{cD} = \Omega_{cH}$). The deuterium distribution function presents a clear fast-ion tail, which is responsible for a substan-

tial increase of the neutron rate. Indeed, the neutron rate synthetic diagnostic built in SSFPQL estimates a neutron rate 4 times higher due to the ICRH than due to the deuterium background alone. This may explain the neutron drop as a redistribution of the energetic deuterium ions created by ICRH second-harmonic heating. In order to fully characterize the orbits of the lost ions and identify the wave-particle resonances responsible for the losses, the phase-space (energy and pitch angle at the FILD position) of the fast-ion losses have been investigated. In the presence of multiple AEs, e.g. t=1.36s, fast-ions are ejected within a broad energy range with gyroradius from $\approx$ 35 mm up to $\approx$ 105 mm. For the magnetic field at the probe, $\approx 1.6T$, this gyroradii range corresponds to hydrogen ions with energies between $\approx$ 0.2 MeV and $\approx$ 1.4 MeV. The velocity-space of lost fast-ions measured by FILD changes strongly during the evolution of the AE activity, showing a completely different pattern within the next 200 ms with fast-ion losses well localized at high pitch angles ($\approx 71^{\circ}$) and energies (gyroradius $\approx$ 60 mm).

A Fourier analysis of the fast-ion loss signal allows to identify the MHD fluctuations responsible for these losses, Fig.3(a). The AC-TAE details of the FILD spectrogram are striking. A clear correlation between the TAE frequency pattern and the fast-ion loss frequencies is observed in both magnetics, Fig.1(b), and FILD, Fig.3(a), spectrograms. Although all TAEs eject resonant ions, the relative amplitude of the measured losses with respect to the fluctuation amplitude does not depend only on the magnetic fluctuation amplitude e.g. the losses measured at the n=4 TAE frequency are not as strong as one could expect from its large fluctuation amplitude in Fig.1(b). Changes in the spatial distribution of the losses could explain this observation as the measurements are performed at a single poloidal position. In addition, fast-ion losses chirping in frequency from approximately the geodesic frequency, f_{AC}^{min}, up to the TAE frequency, f_{TAE}, emerge following the typical AC frequency pattern. The AC induced resonant losses appear stronger ($\approx$ 10 % of the total resonant losses) in the frequency range where the ACs interact with the Alfvén-acoustic branch near the f_{AC}^{min} and during the AC-TAE transition.

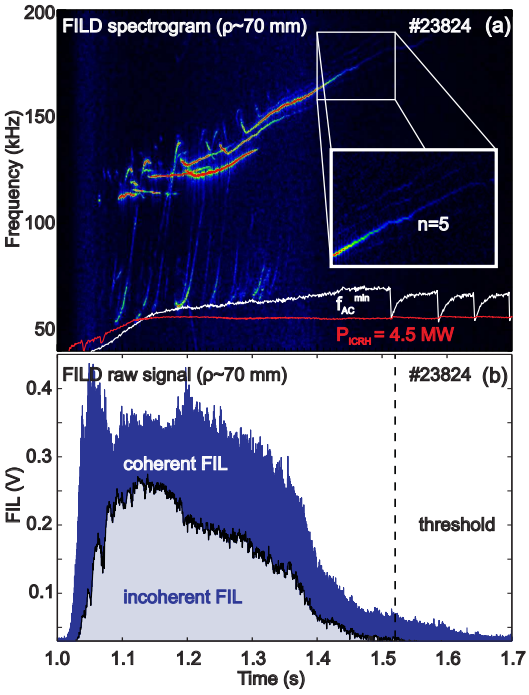

FIG. 3: AUG discharge #23824. (a) spectrogram of the fast-ion loss signal with gyroradius $\approx$ 70mm. The lowest AC frequency, f_{AC}^{min}, is superimposed in white while the total ICRH power(P_{ICRH}) is superimposed in red. The insert shows the single TAE responsible for the onset of the incoherent losses. (b) Fast-ion loss signal. The coherent and incoherent components of the losses are highlighted. The vertical dashed line depicts the threshold for the incoherent losses.

The raw data of the Fourier-analyzed fast-ion loss signal shown in Fig.3(a) is presented in Fig.3(b) to investigate the diffusive and convective character of the losses. The signal consists of a modulated (coherent) signal sitting on an incoherent background whose amplitude varies with time. The coherent component of the fast-ion losses is correlated in frequency and phase with the corresponding magnetic fluctuation, giving rise to the spectrogram shown in Fig.3(a). The incoherent component is dominant, up to 80 % of the total losses, in the presence of multiple frequency chirping AEs, t$\approx$(1.1-1.3)s, and decreases when the number of modes decreases. However it should be noted that it is not

zero when only one mode is ejecting ions with a relatively large amplitude, t≈(1.42-1.52)s, as discussed later. During the time window t≈(1.52-1.65)s only coherent losses induced by a single TAE, n=5, are visible. Going backwards in time, the incoherent losses of ions with gyroradius $\approx 60-70$ mm appear, for t≤1.52s, when the local maximum radial displacement of the magnetic field lines is larger than ≈ 2 mm as measured by its fluctuation induced on the SXR emission. This threshold in the fluctuation amplitude is depicted in Fig.3(b) with a vertical dashed line.

The basic properties of the coherent and incoherent losses are investigated through their dependence on the magnetic fluctuation amplitude. Tracking the frequencies of the individual fluctuations in both, magnetics and FILD spectrograms, we get the relationship between the coherent fast-ion losses and the corresponding magnetic fluctuation amplitude. Fig.4(a) shows this exercise for the TAE n=3 between t=1.24s and t=1.32s. A clear linear dependence is visible during the whole time window, showing the convective character of the underlying loss mechanism. A similar analysis has been done for the incoherent losses shown in Fig.3(b). The envelope of the incoherent losses, black curve in Fig.3(b), is plotted in Fig.4(b) as a function of the amplitude of the TAE n=5 for a time interval close to the onset of the incoherent losses, insert in Fig.4(b), t=(1.42,1.50)s. A clear quadratic dependence has been obtained, strongly suggesting a diffusive mechanism involving several resonances in phase-space. This is supported by the fact that the losses cover a larger domain in velocity-space when the incoherent signal is not zero. It should also be underlined that, as shown in Fig.3(b), the incoherent component is even larger in the presence of several modes, which is also expected to induce a stochastic fast-ion transport.

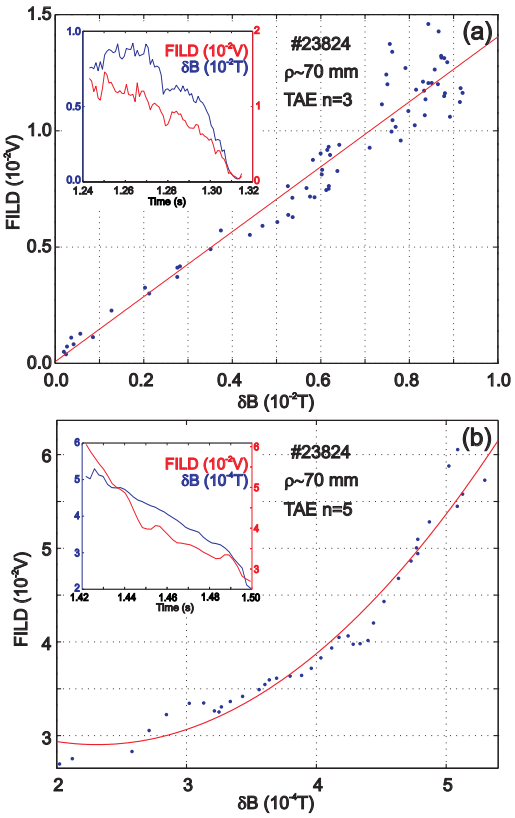

FIG. 4: AUG discharge #23824. Fast-ion loss rate. (a) Linear dependence of the coherent losses at the TAE n=3 frequency on the MHD fluctuation amplitude. (b) Quadratic dependence of the incoherent losses on the TAE n=5 fluctuation amplitude.

Simulations with the full orbit code GOURDON [13] and the guiding center drift orbit code HAGIS [14] have been performed to better understand the nature of the escaping ions and their interactions with the AE waves. Typical orbits of escaping ions detected by the FILD system have been followed backwards in time from the detector to the plasma with the GOURDON code [15]. The possible wave-particle resonances responsible for the fast-ion loss have been investigated in fast-ion phase-space with the HAGIS code [15], [16]. The resulting high density of resonances suggests a stochastic transport though detailed non-linear HAGIS simulations with different q-profiles are underway to estimate the convective and stochastic contribution to the total ion loss.

3. AEs and fast-ion transport in NBI heated discharges

NBI is a standard heating system in present magnetically confined fusion devices. Indeed, in many machines, it is the primary source of auxiliary heating, particles and torque. A thorough understanding of the beam behaviour (deposition profile, steady state fast-particle distribution function, injection energy, etc) is crucial for plasma operation and it is therefore typically available.This information makes the NBI system a reliable tool for quantitative analysis of MHD stability and fast-ion transport to for instance benchmark numerical tools.

3.1. AEs

In AUG, AEs are driven unstable by sub-alfvenic NBI ions during the current ramp-up phase with relative high off-axis minimum of the safety factor. The plasma density is kept at a relatively low value of $\approx 2-3\cdot 10^{19}m^{-3}$, so the fast-ion pressure is a significant fraction of the total plasma pressure. The discharge is initially in limiter configuration and switches to divertor configuration at $t \approx 0.5s$. Throughout the period of interest, the NBI system is injecting deuterium neutrals with a main energy of 60 keV thus producing sub-alfvenic deuterium ions. In the first 550 ms a large number of RSAEs in the frequency range between ≈ 30 and ≈ 200 kHz are observed by the ECEI system, see Fig.5(a). The RSAE activity is abruptly stopped by a sawtooth-like crash which causes an electron temperature drop of ≈ 30 % with little change in the density profile. It is important to remark that no fluctuation monitor has detected any TAE fluctuation in this discharge. Indeed, the fast-particle source (NBI beam) has to be replaced with a different beam with similar injection geometry and higher full-energy (93 keV) to drive TAEs unstable. Several RSAEs and TAEs are then clearly visible in the magnetic power spectrogram (Fig.6(e)) while the ECEI crosspower spectrogram shows RSAEs in the frequency range between ≈ 60 kHz and ≈ 200 kHz.

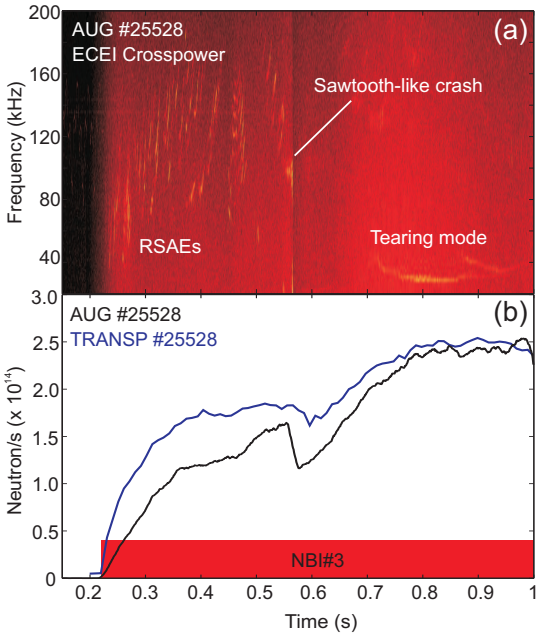

FIG. 5: AUG discharge #25528. (a) Crosspower of the NBI driven AE electron temperature fluctuation measured by the ECE imaging system. (b) Temporal evolution of the measured (black) and predicted by TRANSP (blue) neutron rates.

3.2. Fast-ion transport

In the presence of NBI driven AEs a clear deficit of neutrons is observed when comparing the measured neutron rates with that predicted by TRANSP. In discharge #25528, the neutron rate steadily increases throughout the current ramp as soon as the NBI is switched on. TRANSP predicts (blue time trace in Fig.5(b)) a neutron rate of up to ≈ 40 % higher then the measured one (black time trace in fig5(b)). As the RSAEs dissapear the measured neutron rate starts recovering, matching the classical rate predicted by TRANSP when no MHD activity is present in the plasma at t ≈ 1.0 s. The fast-ion density profile measured (black crosses in Fig.6(a)) by the recently developed in AUG FIDA technique [17] presents a clear depletion in the central fast-ion population when many RSAEs are unstable at the same time, $t \approx 0.475s$, while at $t \approx 1.0s$

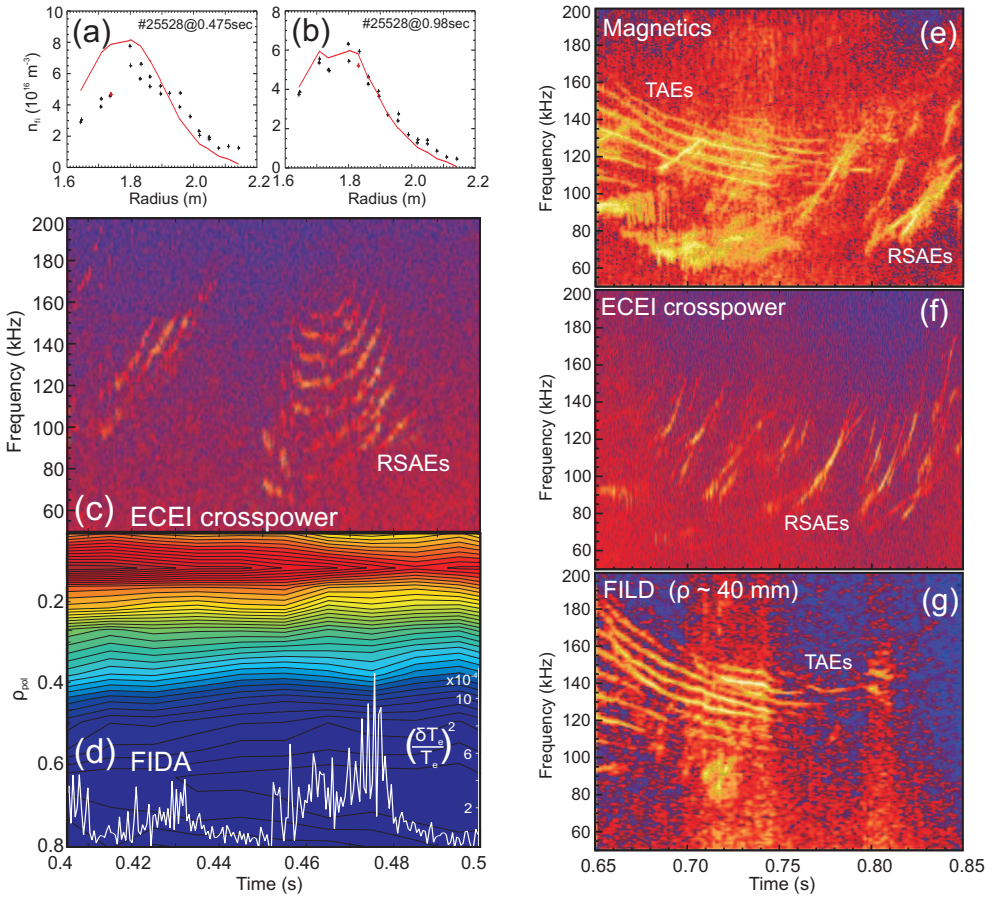

FIG. 6: NBI driven AEs and subsequent fast-ion transport. (a)-(d) AUG discharge #25528. FIDA profiles at (a) t=0.475 s and (b) t=0.98 s. In red the FIDA profiles calculated with the FIDASIM code using measured kinetic profiles and classical fast-ion profiles predicted by TRANSP. (c) ECEI crosspower spectrogram and (d) temporal evolution of the FIDA density profile and of the global RSAE amplitude (white curve). (e)-(g) AUG discharge #25491. Power spectrograms of (e) a magnetic pick-up coil, (f) the electron temperature fluctuation measured by the ECEI system and (g) of the fast-ion losses measured by FILD.

(Fig.6(b)) both, measured (black crosses) and simulated profiles (red) are in excellent agreement. The classical profiles shown in red in Figs.6-(a) and -(b) have been simulated using the FIDASIM code [18] taking the actual plasma parameters and the classical fast-ion distribution functions predicted by TRANSP. Fig.6(d) shows the temporal evolution of the FIDA density profile during the RSAE activity. The FIDA profile temporal evolution shows an extra drop of the central fast-ion density, as q_{min} passes through an integer (as the simultaneous occurrence of many RSAEs indicates), correlated with the maximum of a global RSAE fluctuation amplitude (white curve in Fig.6(d)). The temporal evolution of the global RSAE fluctuation amplitude has been calculated by summing over all RSAE temperature fluctuations detected by the ECEI. It is important to remark that no fast-ion losses have been observed so far in AUG discharges with the solely detectable presence of NBI driven RSAEs. In fact, when many RSAEs and TAEs are unstable at the same time, the coherent fast-ion losses are dominated by the radially extended TAEs while only strong RSAEs cause some coherent fast-ion losses as Fig.6(e)-(g) show. Detailed simulations with realistic first wall geometry, eigenmode structures and fast-ion distributions are necessary to decouple first-order geometric from non-linear wave-particle interaction effects.

4. Conclusions

The confinement of both trapped and passing ions of RF and NBI origin has been observed to be strongly affected by AEs. Convective and diffusive fast-ion losses induced by AEs have been measured at the plasma edge. Diffusive losses are observed with a single TAE causing coherent losses above a certain threshold in the local fluctuation amplitude. The temporal evolution of the fast-ion profile has been monitored using the FIDA technique. A large drop in the central fast-ion density due to many RSAEs as q_{min} passes through an integer has been observed. In general, radially extended TAEs are more efficient ejecting ions from the plasma than RSAEs while the latter may act as a fast-ion seed, redistributing the ions from the plasma core to the TAE area of influence, modifying considerably the fast-ion spatial gradients.

References

[1] HEIDBRINK, W. W., Phys. Plasmas **15** (2008) 055501.
[2] FASOLI, A. et al., Nucl. Fusion **47** (2007) S264.
[3] CLASSEN, I. et al., accepted in Rev. Sci. Instrum. (2010).
[4] GARCIA-MUNOZ, M. et al., Rev. Sci. Instrum. **80** (2009) 053503.
[5] HEIDBRINK, W. W. et al., Plasma Phys. Controlled Fusion **46** (2004) 1855.
[6] GARCIA-MUNOZ, M. et al., Phys. Rev. Lett. **104** (2010) 185002.
[7] GARCIA-MUNOZ, M. et al., Phys. Rev. Lett. **100** (2008) 055005.
[8] CHENG, C. and CHANCE, M., J. Comput. Phys. **71** (1987) 1124.
[9] BREIZMAN, B. N. et al., Phys. Plasmas **12** (2005) 112506.
[10] VAN-ZEELAND, M. A. et al., Phys. Rev. Lett. **97** (2006) 135001.
[11] SASSENBERG, K. et al., Plasma Phys. Control. Fusion **51** (2009).
[12] BRAMBILLA, M., Plasma Phys. Control. Fusion **41** (1999) 1.
[13] GOURDON, C., *Programme optimise de calculs numeriques dans les configurations magnetiques*, Centre d'etudes nucleaires de Fontenay aux Roses, 1970.
[14] PINCHES, S. D., Comput. Phys. Commun. **111** (1998) 131.
[15] GARCIA-MUNOZ, M. et al., Nuclear Fusion **50** (2010) 084004.
[16] LAUBER, P. et al., IAEA-CN-180/THW/2-2Ra (2010).
[17] GEIGER, B. et al., in preparation (2010).
[18] HEIDBRINK, W. W. et al., submitted to Communications in Computational Physics (2010).